Supporting Information

Branchpoint expansion in a fully-complementary three-way DNA junction

Tara Sabir,[1,2] Anita Toulmin,[1,2] Long Ma,[3] Anita C. Jones,[3] Peter McGlynn,[4] Gunnar F. Schröder,[5]* and Steven W. Magennis[1,2,]*

[1]The School of Chemistry, The University of Manchester,

Oxford Road, Manchester, M13 9PL, UK

[2]The Photon Science Institute, The University of Manchester,

Alan Turing Building, Oxford Road, Manchester, M13 9PL, UK

[3]EaStCHEM School of Chemistry and Collaborative Optical Spectroscopy, Micromanipulation and Imaging Centre, The University of Edinburgh, West Mains Road, Edinburgh, EH9 3JJ, UK

[4]Institute of Medical Sciences, University of Aberdeen, Ashgrove Road West, Aberdeen, AB25 2ZD, UK

[5]Institute of Complex Systems (ICS-6), Forschungszentrum Jülich, 52425 Jülich, Germany

Supporting Materials and Methods

a) Preparation of DNA duplexes and branched DNA structures

Oligonucleotides were synthesised and labeled by Purimex GmbH (Grebenstein, Germany). The NHS-esters of Alexa488 (5'/6' mixed isomer, Invitrogen) or Cy5 (GE-Healthcare) were attached via a 5-C_6-aminoallyl-deoxythymidine. Annealing of samples for branched DNA was carried out in buffer (13 mM Tris, 65 mM NaCl, pH 7.5). Annealing buffer for duplexes contained 16 mM Tris and 80 mM NaCl. For all structures the ratio of donor strand to other strands was 1:3. Samples were heated to 90 °C in a water bath and left to cool slowly overnight. For measurement, all samples were diluted into buffer containing 20 mM Tris, 15 mM NaCl and 1 mM ascorbic acid. Prior to sample addition, the buffer was stirred with activated charcoal to remove fluorescent impurities. The measurement buffer contained either 0 mM or 1 mM $MgCl_2$.

For the 2-aminopurine samples, oligonucleotides were synthesised by Purimex GmbH (Grebenstein, Germany). The protocol was the same as above and used the 2-AP phosphoramidite for labelling (Glen Research). Annealing of samples was carried out in buffer (20 mM Tris, 15 mM NaCl pH 7.5). The ratio of 2-AP labeled oligonucleotides to non-labeled DNA was 1:3 for all structures. Samples were heated to 90°C in a water bath and left to cool overnight. For measurements, samples were diluted into buffer (20mM Tris, 15mM NaCl, pH 7.5).

b) Sequences of oligonucleotides

Oligonucleotides for FRET studies. In addition to the sequences used for the 3WJ (shown in Figure 1a), two duplexes were prepared as control samples: AT1-AT2 and AT4-AT5. The sequences of the oligonucleotides are shown below.

AT1 5’ TAT CAT AAA TAA ATG GTA TAT T(Alexa488)TT ATA ACT 3’

AT2 5’ AGT TAT AAA ATA TAC CAT TTA T(Cy5)TT ATG ATA 3’

AT4 5’ CAT TAT AAA TAA ATG GTA TAT TTA AT(Alexa488)A ATC 3’

AT5 5’ GAT TAT TAA ATA TAC CAT TTA TTT AT(Cy5)A ATG 3’

Oligonucleotides for 2-AP studies. Seven oligonucleotides with the same sequences as those used for the 3WJ in FRET studies (Figure 1a), were labelled in a single position with 2-AP (labelling position indicated by X).

Pos. 1 5' GTC GGA TCC TCT XGA TAT CTC CAT GCT CAC TGG TTA TAG GAG AAT CCG GG

Pos. 2 5' GTC GGA TCC TCT AGA TAT CTC CXT GCT CAC TGG TTA TAG GAG AAT CCG GG

Pos. 3 5' AAT CTC ACA GCT GAT CACATT GCT XCA TGG AGA TAT CTA GAG GAT CCG AC

Pos. 4 5' AAT CTC ACA GCT GAT CXCATT GCT ACA TGG AGA TAT CTA GAG GAT CCG AC

Pos. 5 5' CCC GGA TTC TCC TXT AAC CAG TGA GTA GCA ATG TGA TCA GCT GTG AGA TT

Pos. 6 5' CCC GGA TTC TCC TAT AAC CAG TGX GTA GCA ATG TGA TCA GCT GTG AGA TT

Pos. 7 5' CCC GGA TTC TCC TAT AAC CAG TGA GTA GCA ATG TGA TCX GCT GTG AGA TT

A composite picture showing the sequence of the 3WJ and labelling positions is found in Figure 3a. The duplex controls were formed from the single strands above, and the complementary, unlabelled 50mer strand (sequence not shown).

c) Ensemble optical spectroscopy of FRET samples. Absorption spectra were measured on a Perkin Elmer Lambda 1050 spectrometer. Corrected fluorescence emission spectra were collected, under magic angle conditions, using a Fluorolog spectrometer (HORIBA Jobin Yvon) with R928P PMT. The absorbance of the sample was low (< 0.05) so that inner-filter effects were negligible.

d) Single-molecule multi-parameter fluorescence detection (MFD) and calculation of FRET distances. MFD is based around burstwise detection of fluorescence as single molecules diffuse through the focus of a confocal microcope. Photon counting detection by multiple detectors allows simultaneous detection of the color, lifetime, polarisation and intensity of fluorescence for each molecule.[1] MFD measurements were performed using a home-built system, which we described previously.[2] The process for calculating the FRET distances from the MFD data was described previously.[2] The FRET distances reported here were reproducible to ≤2 Å standard deviation.

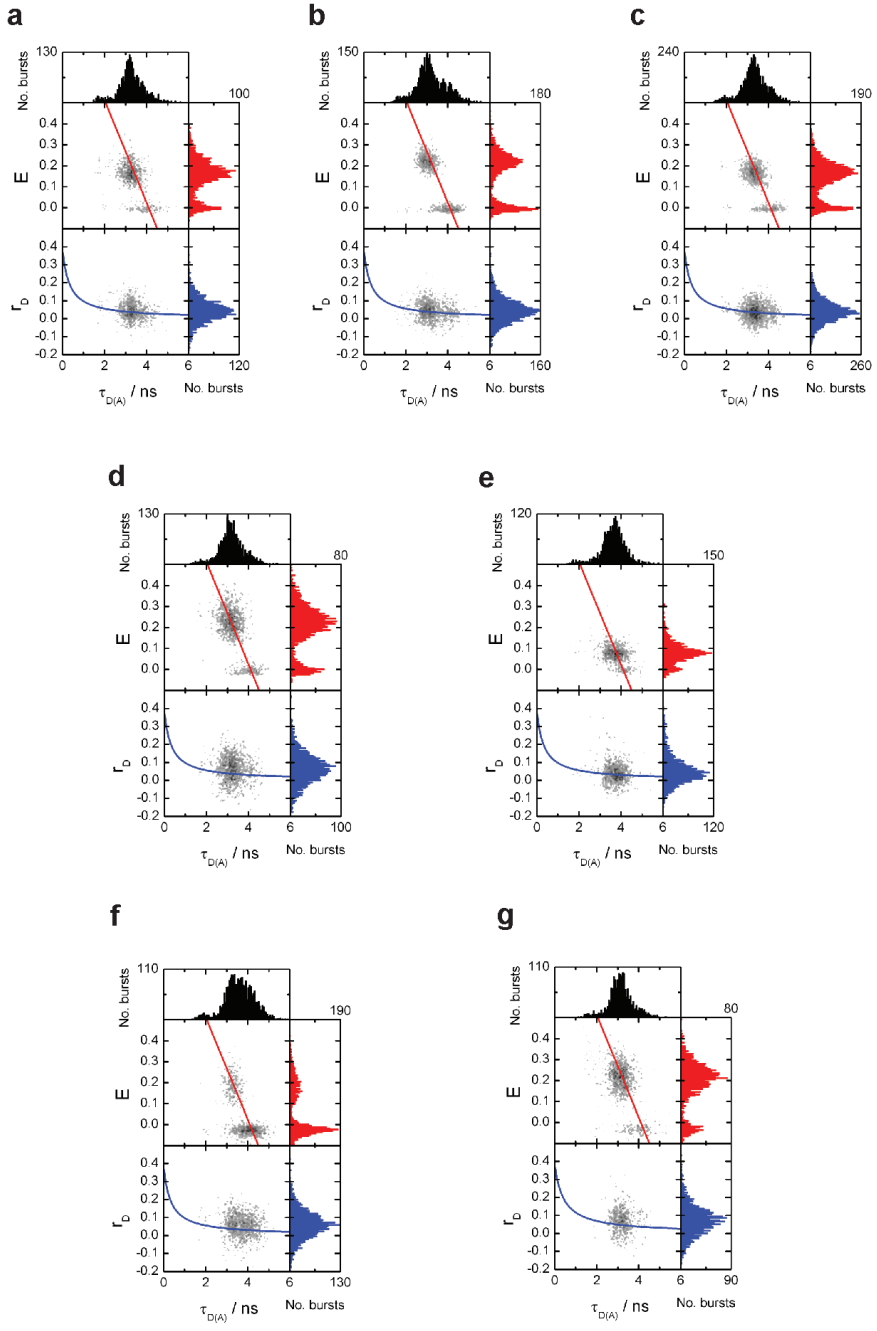

Figure S1. Single-molecule FRET for the 3WJ. The 2D plots are of FRET efficiency (E) and donor anisotropy (r_D) versus donor lifetime ($\tau_{D(A)}$), as described in Figure 1. Typical data are shown for all seven FRET pairs: (a) D1A1, (b) D1A2, (c) D1A3, (d) D2A1, (e) D2A3, (f) D3A1 and (g) D3A2. The sample buffer contained 1 mM Mg^{2+}.

e) Molecular Dynamics (MD) Simulations. For the starting model, the three DNA arms of the three-way junction were modeled as B-DNA using the program Hyperchem (Version 8.0.8 for Windows, Molecular Modeling System, Lightwave Scientific). The program CNS[3] was then used for the simulated annealing molecular dynamics calculation.

During the simulation, FRET distance restraints were applied to model the geometry of the DNA. We used the mean dye positions for Alexa488 and Cy5 obtained from a MD simulation that has been published previously.[4] To assess the accuracy of the distance measurement, we studied two different duplexes, AT1-2 and AT4-5 (see above for sequences), labelled with the same dyes, Alexa488 and Cy5, used for the 3WJ experiments. The MFD plots are shown in Figure S2. These are qualitatively similar to that for the 3WJ (see Figure 1b). We then calculated the distance from the FRET efficiency, as described above, and compared this with the distance between mean dye positions, assuming a model B-DNA duplex structure. The experimental distances were 59±1 Å for AT1-2 and 79±1 Å for AT4-5, while the distances for model B-DNA were 56 Å and 78 Å for AT1-2 and AT4-5, respectively.

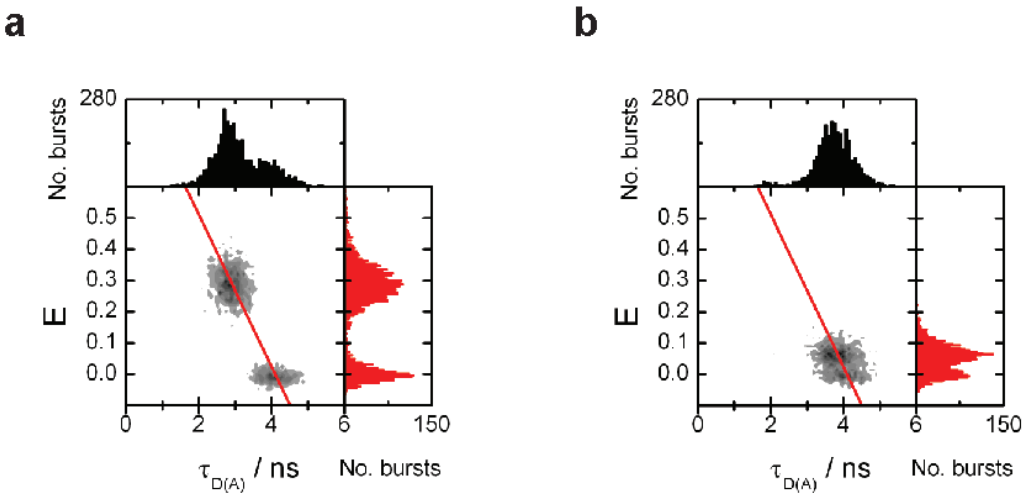

Figure S2. Single-molecule FRET for duplex DNA controls AT1-AT2 (a) and AT4-AT5 (b). The 2D plots are of FRET efficiency (E) versus donor lifetime ($\tau_{D(A)}$). The gray scale indicates an increasing number of single-molecule bursts (from white to black). Also shown are the corresponding 1D histograms. FRET efficiencies were measured from raw green and red signals and corrected for background (1.21 kHz in green; 2.13 kHz in red), spectral crosstalk (4.1%), detection efficiencies (green:red = 0.3) and the fluorescence quantum yields (0.80 for donor; 0.32 for acceptor). The red overlaid line is the theoretical FRET relationship, $E = 1 + \tau_D/\tau_{D(A)}$), with $\tau_D = 4.1$ns. The samples were measured in the 0 mM Mg^{2+} buffer.

For the 3WJ, the mean positions were fixed relative to the surface of the DNA by distance restraints. The distance restraints were generated by the new DEN (Deformable Elastic Network) feature[5] in CNS which selects random atom pairs that are within a specified distance range in the starting structure. It should be noted that we did not actually use deformable restraints, but rather used regular (non-deformable) harmonic distance restraints during the refinement. For each dye atom, pairs were randomly

selected from within 15Å of the dyes yielding on average 36 distance restraints per dye.

To maintain the B-DNA conformation of the arms during the simulated annealing procedure, additional restraints were generated for the bases: 7144 atom pairs that are within a distance range of 15Å were randomly selected from the group of atoms that belong to the bases. However, for the 2-free case, two pairs of bases in each arm that are closest to the branch-point (12 bases in total) were left unrestrained to avoid artifacts from enforcing B-DNA conformation in the branch region. Similarly, for the 0-free case all bases were restrained, for the 1-free case one base pair per arm next to the branchpoint was left unrestrained (6 bases in total), and for the 3-free case the 18 bases closest to the branchpoint were left unrestrained. The elastic restraints were made non-deformable by using a DEN gamma parameter of zero. The starting temperature for the simulated annealing simulation was 3000 K and decreased to 0 K within 15 ps.

For both sets of FRET distances (corresponding to 0 mM and 1 mM Mg^{2+}), 50 simulated annealing runs with different initial velocities were performed. The distance root mean square deviation (DRMSD) between the FRET distances and the dye positions in the model measures how well the model fits the measured FRET distances. The 50 models generated for the 2-free case in low and high salt buffer are shown in Figure S3. It is clear that the structures are confined to a narrow range of conformations.

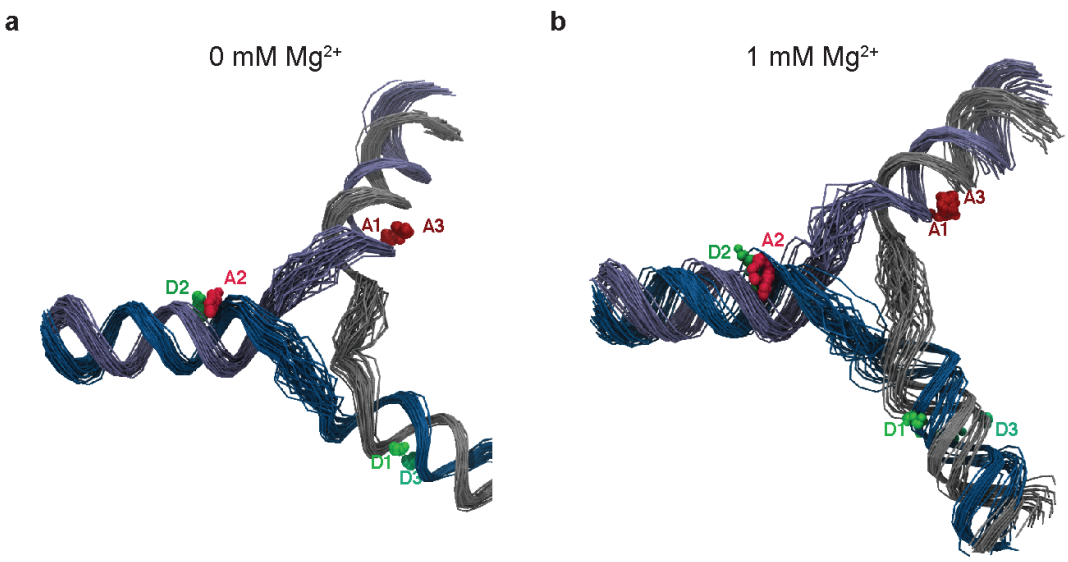

Fig. S3. Overlay of all 50 structures generated by MD for the 3WJ in low salt (a) and high salt buffer (b), with "2-free" restraints applied. See text for details.

Testing the structural model. As described in the main text, four different sets of restraints were tested: all base pairs restrained (0-free), and one, two or three base pairs per arm left unrestrained (1-free, 2-free and 3-free, respectively). The DRMSD values are shown in Table S1. An overlay of the 50 solution structures for 3WJ in 0 mM $MgCl_2$ for the 0-free, 1-free and 2-free cases is shown in Figure S4. As described above, our experimental distance measurements are in good agreement with modelled distances in DNA. To test for the effects of small systematic errors in the structural determination, we also modelled the 3WJ (2-free case) with all FRET distance restraints offset by ± 1 Å. The results are shown in Figure S5. There are only minor changes to the structures, showing that our conclusion regarding the local and global structure of the 3WJ would be unaffected by minor systematic errors.

Table S1. DRMSD for different branchpoint restraints

Restraint	DRMSD in 0 mM Mg^{2+} / Å	DRMSD in 1 mM Mg^{2+} / Å
0-free	1.68	2.13
1-free	0.89	0.91
2-free	0.59	0.64
3-free	0.62	0.55

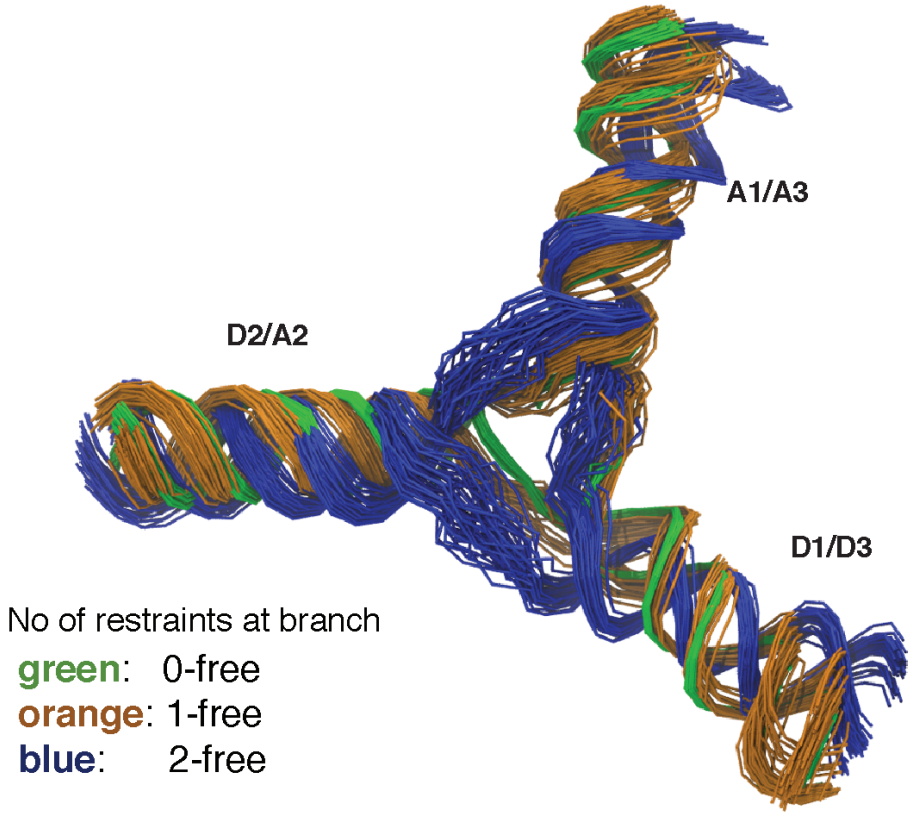

Figure S4. Effect of restraints at branchpoint for 3WJ in 0mM Mg^{2+} buffer. See text for details.

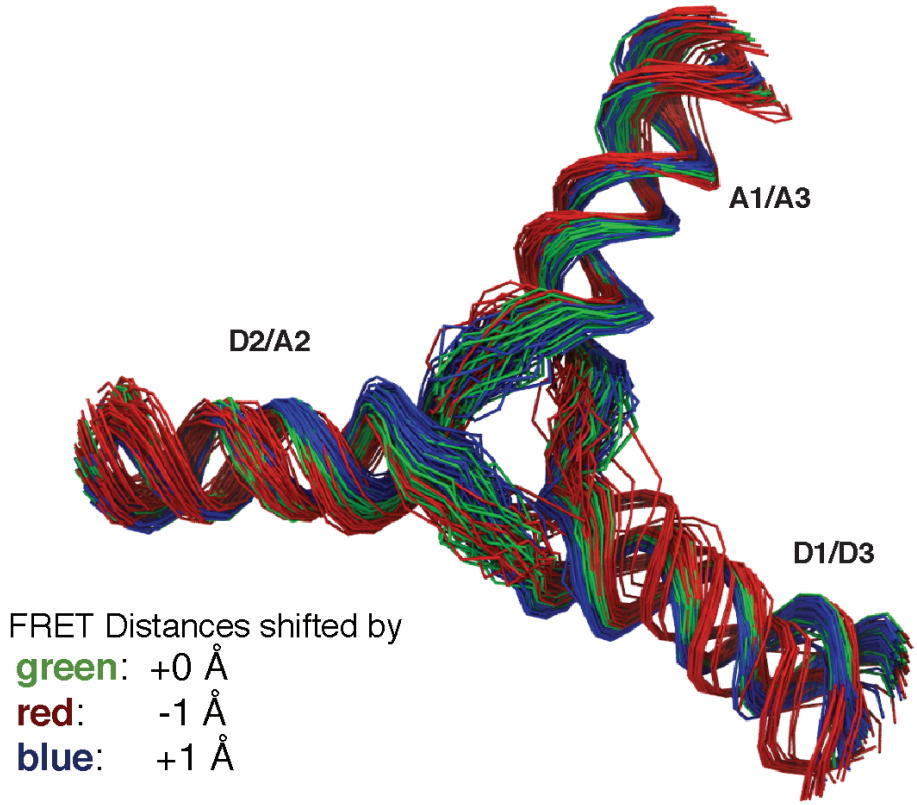

Figure S5. Effect of small systematic changes in FRET restraints for 3WJ in 0mM Mg^{2+} buffer. See text for details.

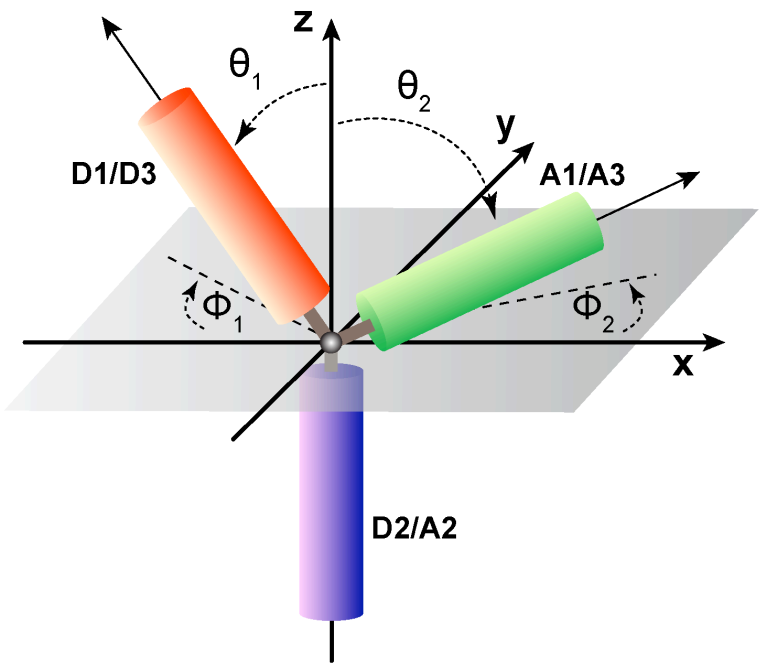

Figure S6. Geometric model of a 3WJ where the global structure is defined by the polar angles, θ and ϕ. The dyes (D and A) attached to each arm are indicated and correspond to the structures shown in Figure 1a.

f) Time-resolved fluorescence spectroscopy of 3WJs labeled with 2-AP

Decay curves were analyzed using a standard iterative reconvolution method, assuming a multiexponential decay function.

$$I(t) = \sum_{i=1}^{n} A_i \exp\left(\frac{-t}{\tau_i}\right)$$

where A_i is the fractional amplitude and τ_i is the fluorescence lifetime of the i^{th} decay component. Fluorescence decay curves at three emission wavelengths (370, 380 and 390 nm) were analyzed globally using Edinburgh Instruments 'FAST' software, *i.e.* they were fitted simultaneously, with lifetimes, τ_i, as common parameters.

The fitted data for 2-AP in positions 2-6 for ssDNA, duplex DNA and 3WJ are shown in Table S2. Figure S7 shows plots of the product of A-factor and lifetime ("A×Tau") for each of the four lifetime components in Table S2. As highlighted in Figure S8, lifetime component 3 (highlighted in blue) is much increased in ssDNA (>0.3) compared to duplex DNA and the 3WJ, while components 3 and 4 are much greater than components 1 and 2. For the 3WJ, when 2-AP is in positions 2, 4 and 5 (J2, J4, J5), the plots resemble those of the duplex. In contrast, J3 shows a greatly-increased component 3, in comparison with the corresponding duplex, indicative of unpairing. Similarly, J6 also has a high component 3, almost as high as in the ssDNA sample, with components 3 and 4 much greater than components 1 and 2, as observed for ssDNA.

Table S2. Fluorescence lifetimes (τ_i) and their fractional amplitudes (A_i) for ssDNA, dsDNA and 3WJ. Data are shown for 2-AP in positions 2-6, corresponding to the positions indicated in Figure 3 and in the Supporting Information above.

ssDNA	τ_1/ns	τ_2/ns	τ_3/ns	τ_4/ns	A_1	A_2	A_3	A_4
Pos. 2	0.07	0.58	2.2	6.8	0.67	0.15	0.14	0.04
Pos. 3	0.09	0.55	2.2	6.1	0.66	0.16	0.14	0.04
Pos. 4	0.10	0.63	2.5	7.4	0.59	0.19	0.16	0.06
Pos. 5	0.06	0.53	2.1	5.4	0.65	0.13	0.18	0.04
Pos. 6	0.07	0.69	2.9	7.6	0.64	0.14	0.15	0.08

dsDNA	τ_1/ns	τ_2/ns	τ_3/ns	τ_4/ns	A_1	A_2	A_3	A_4
Pos. 2	0.05	0.37	2.7	10.6	0.87	0.08	0.03	0.02
Pos. 3	0.10	0.35	2.4	9.7	0.90	0.07	0.02	0.01
Pos. 4	0.04	0.38	2.8	10.5	0.76	0.17	0.05	0.02
Pos. 5	0.08	0.35	2.5	9.1	0.55	0.41	0.03	0.01
Pos. 6	0.07	0.45	2.6	8.8	0.68	0.18	0.09	0.05

3WJ	τ_1/ns	τ_2/ns	τ_3/ns	τ_4/ns	A_1	A_2	A_3	A_4
Pos. 2	0.05	0.47	2.4	10.1	0.82	0.10	0.06	0.02
Pos. 3	0.08	0.45	2.2	8.1	0.76	0.13	0.09	0.02
Pos. 4	0.06	0.50	2.4	9.5	0.73	0.15	0.10	0.02
Pos. 5	0.08	0.38	2.1	7.9	0.62	0.30	0.06	0.01
Pos. 6	0.07	0.59	2.9	9.1	0.67	0.16	0.14	0.04

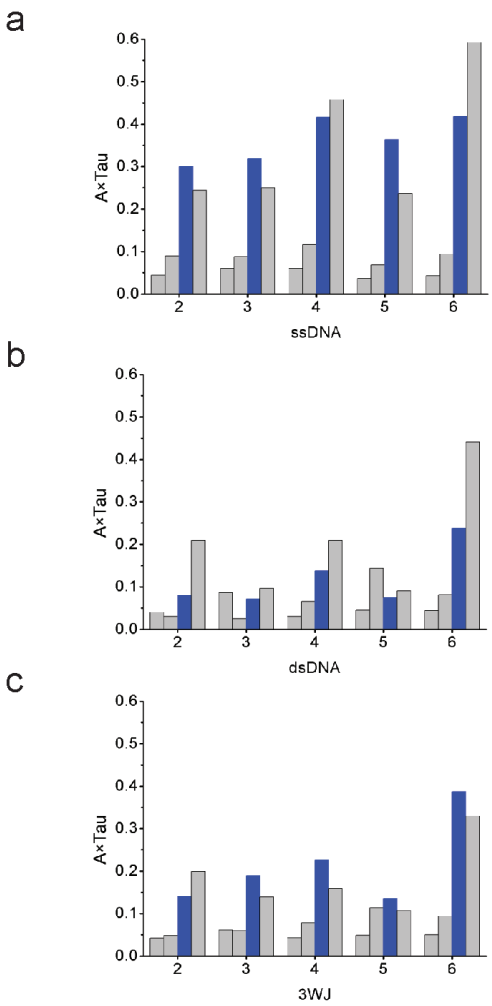

Figure S7. Plots of the product of A-factor and lifetime ("A×Tau") for each of the four lifetime components fitted to 2-AP fluorescence decays in ssDNA (*A*), duplex DNA (*B*) and 3WJ (*C*) for labeling positions 2-6. The components are displayed with increasing lifetime from left to right, corresponding to τ_1-τ_4 in Table S2. Component three is highlighted in blue. The labeling positions are illustrated in Figure 3a.

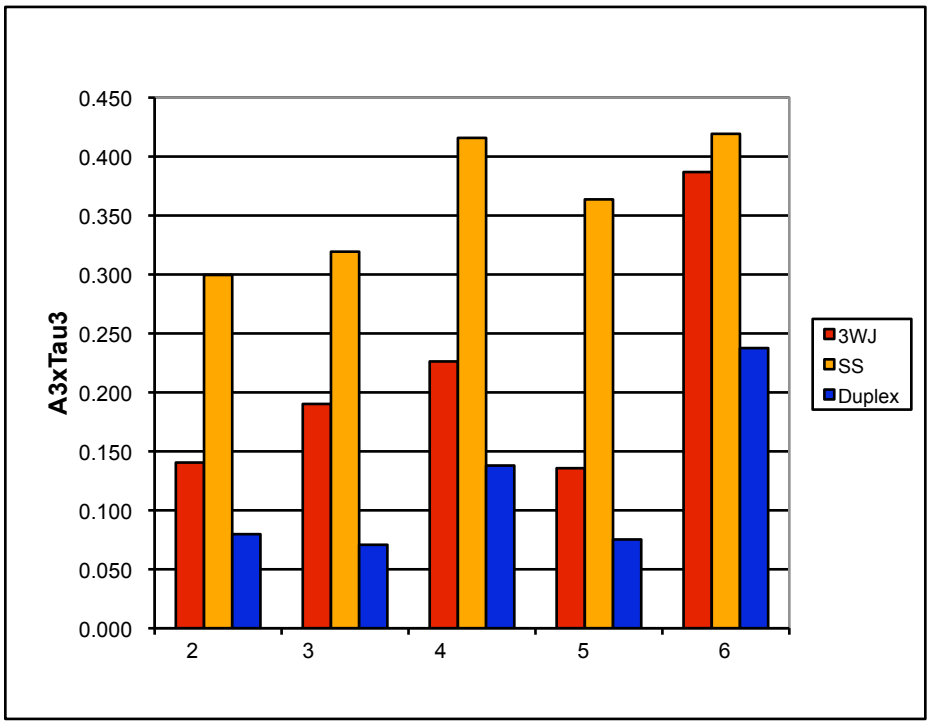

Figure S8. Comparison of the product of A-factor and lifetime ("A×Tau") for lifetime component 3 (see TableS2 and Figure S7) in ssDNA (orange), duplex DNA (blue) and 3WJ (red) for labeling positions 2-6.

References

1. Rothwell, P. J.; Berger, S.; Kensch, O.; Felekyan, S.; Antonik, M.; Wohrl, B. M.; Restle, T.; Goody, R. S.; Seidel, C. A. M. *Proc. Natl. Acad. Sci. USA* **2003**, *100*, 1655-1660.
2. Sabir, T.; Schröder, G. F.; Toulmin, A.; McGlynn, P.; Magennis, S. W. *J. Am. Chem. Soc.* **2011**, *133*, 1188-1191.
3. Brunger, A. T. *Nat. Protoc.* **2007**, *2*, 2728-2733.
4. Woźniak, A. K.; Schröder, G. F.; Grubmüller, H.; Seidel, C. A. M.; Oesterhelt, F. *Proc. Natl. Acad. Sci. USA* **2008**, *105*, 18337-18342.
5. Schröder, G. F.; Brunger, A. T.; Levitt, M. *Structure* **2007**, *15*, 1630-1641.